A Letters Journal Exploring the Frontiers of Physics

January 2014

EPL, **105** (2014) 24001 www.epljournal.org
doi: 10.1209/0295-5075/105/24001

Dynamics of snapping beams and jumping poppers

A. Pandey[1], D. E. Moulton[2], D. Vella[2] and D. P. Holmes[1(a)]

[1] *Department of Engineering Science and Mechanics, Virginia Polytechnic Institute and State University Blacksburg, VA, 24061, USA*
[2] *Mathematical Institute, University of Oxford - Woodstock Rd, Oxford, OX2 6GG, UK*

received 11 October 2013; accepted in final form 10 January 2014
published online 10 February 2014

PACS 46.32.+x – Static buckling and instability
PACS 46.70.De – Beams, plates and shells
PACS 62.20.D- – Elasticity

Abstract – We consider the dynamic snapping instability of elastic beams and shells. Using the Kirchhoff rod and Föppl-von Kármán plate equations, we study the stability, deformation modes, and snap-through dynamics of an elastic arch with clamped boundaries and subject to a concentrated load. For parameters typical of everyday and technological applications of snapping, we show that the stretchability of the arch plays a critical role in determining not only the post-buckling mode of deformation but also the timescale of snapping and the frequency of the arch's vibrations about its final equilibrium state. We show that the growth rate of the snap-through instability and its subsequent ringing frequency can both be interpreted physically as the result of a sound wave in the material propagating over a distance comparable to the length of the arch. Finally, we extend our analysis of the ringing frequency of indented arches to understand the "pop" heard when everted shell structures snap-through to their stable state. Remarkably, we find that not only are the scaling laws for the ringing frequencies in these two scenarios identical but also the respective prefactors are numerically close; this allows us to develop a master curve for the frequency of ringing in snapping beams and shells.

Introduction. – Arched structures have been used in architecture for over four thousand years [1], and the stability of these bistable structures has captivated scientists for over a century [2,3]. The use of arches in engineering environments has traditionally placed a substantial focus on predicting the onset of loss of stability, and the subsequent unstable modes of deformation [4–9]. More recently, the potential utility of controlling structural stability loss to take advantage of the rapid transition between two stable shapes has been the focus of study. Not only can a large deformation be achieved quickly, but frequently with little energetic cost. Nature has long made use of such elastic instabilities for functionality, with the carnivorous waterwheel plant [10] and Venus flytrap [11,12] using their elaborate snapping leaves to rapidly capture their prey. Meanwhile, snapping shells have captivated children for decades in the form of bimetallic "jumping" disks [13] and rubber toy "poppers" [14,15] that, having first been turned "inside-out" leap from a table with an audible pop as they return to their stable state (see fig. 1). These same principles have recently been used in the development of switches within MEMS devices [16,17], biomedical valves [18], switchable optical devices [19], responsive hydrogels [20], and aerospace engineering [21,22].

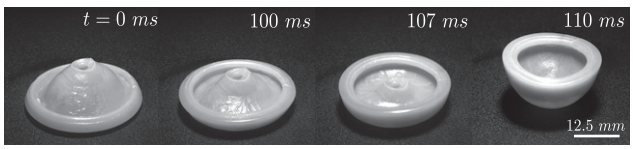

Fig. 1: Snap-through of a commercially available child's popper ($E \approx 25\,\mathrm{MPa}$ and $\rho \approx 1200\,\mathrm{kg/m^3}$) from a flat surface (see the supplementary movie `sample-video1.avi`).

Traditionally, studies of snapping have focussed on the conditions under which a shell or deformed beam can remain in equilibrium [11,23]. Previous work on dynamic buckling tends to focus on how the critical load to induce snapping depends on the dynamics of loading [24,25]. However, in the design of advanced materials an understanding of the dynamics of snapping itself is necessary to make full use of the snapping transition. In this letter, we study the dynamics of snapping using a combination of experiments and theoretical calculations.

(a) E-mail: dpholmes@vt.edu

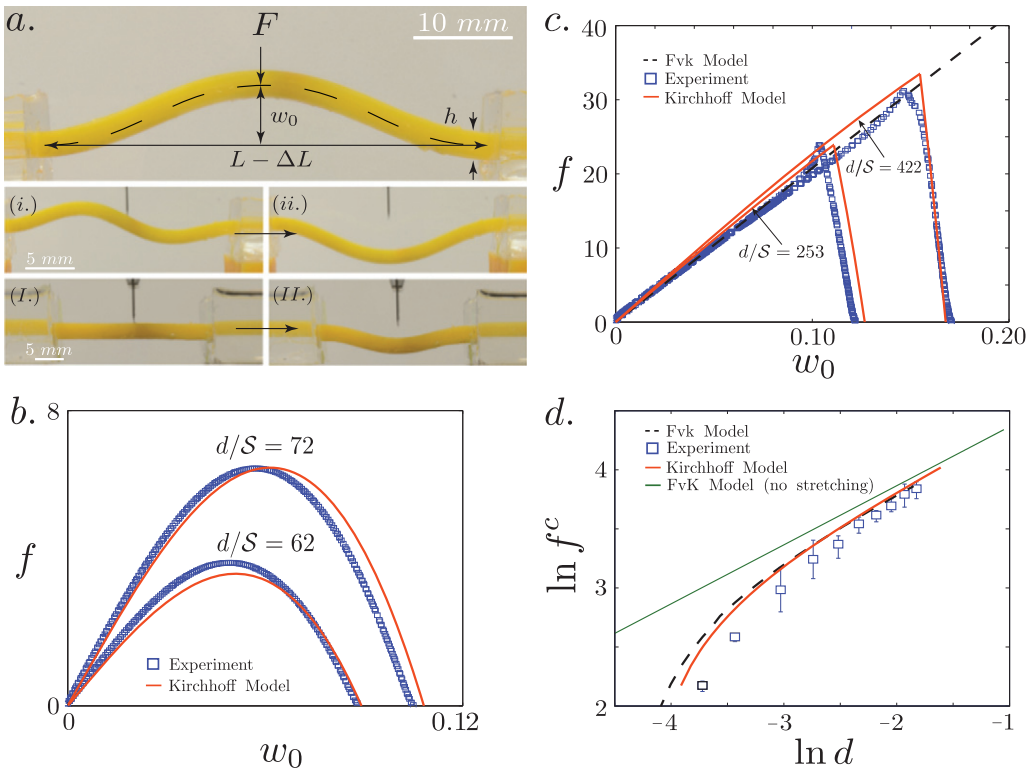

Fig. 2: (Colour on-line) Snap-through of a two-dimensional arch loaded along a line (see the supplementary movie `sample-video2.avi`). (a) Experimental set-up showing a Polyvinylsiloxane (PVS) arch with both ends clamped and loaded at its apex by a razor blade. (i) and (ii) show the asymmetric deformation mode of a deep arch and the subsequent snap-through to the inverted stable configuration. (I) and (II) show a shallow arch going through a flat mode of deformation and snapping. Force-displacement plots for arches that remain symmetric throughout (b) and first deform symmetrically but then asymmetrically (c). (d) Maximum force f^c as a function of end-end compression d for stretchability $\mathcal{S}_1 = 1.912 \times 10^{-4}$.

Experiments. – Motivated by the "snap-through" of a popper shown in fig. 1, we first study the snapping dynamics of a much simpler system: a two-dimensional elastic arch subject to a point load. We consider a shallow arch loaded by a point at its apex, and demonstrate the importance of the beam's "stretchability" on both the form of deformation and the snapping dynamics. In contrast to recent work that has focused on snapping induced by a fixed load [25,26], we consider the limit of "displacement control".

Figure 2(a) illustrates the setup considered here: a clamped beam of length L, thickness h, and width b is compressed by an axial displacement ΔL so that it buckles into an arch. An imposed displacement is then applied as a line load to the mid-point between the two clamped ends[1]. The initial height of the apex before indentation is w_0. Qualitatively speaking, we observe that for shallow arches, the beam remains symmetric about its center throughout the loading (fig. 2(a)I), while deep arches transition from a symmetric to an asymmetric shape well before snap-through occurs (fig. 2(a)i). In both cases, once the neutral axis of the beam is displaced to the mid-point of the clamped edges, global stability is lost, and the beam undergoes rapid snap-buckling to an inverted arch. To understand these observations, we begin by considering the motion before snapping, which we assume is quasi-static, before moving on to study the dynamics of snapping and ringing.

We model the shape of the deformed beam using both the Kirchhoff equations for elastic rods and the Föppl-von Kármán (FvK) equations [27]. In the following discussion, we shall present the results of the FvK theory since this more easily allows for the identification of the important parameters and the calculation of asymptotic results. However, numerical results from the Kirchhoff theory are used in comparisons with experiment since these account correctly for the effect of large displacements.

FvK model. – In the case of small transverse displacement, the profile of the arch is denoted by $w(x,t)$, which satisfies the dimensionless dynamic beam equation [27]

$$\frac{\partial^2 w}{\partial t^2} + \frac{\partial^4 w}{\partial x^4} + \tau^2 \frac{\partial^2 w}{\partial x^2} = f\delta(x), \quad -1/2 < x < 1/2. \quad (1)$$

[1]Polyvinylsiloxane (PVS, Elite 22, Zhermack^{TM}, E = 789.49 kPa) beams were prepared with stretchability $\mathcal{S}_1 = 1.912 \times 10^{-4}$ and $\mathcal{S}_2 = 9.706 \times 10^{-4}$. The ends of the beam were clamped by embedding them within crosslinked polydimethylsiloxane (PDMS) (Dow corning Sylgard 184^{TM}). The indentation was performed in an Instron 5848 Microtester and the force was measured by Interface ULC 0.5 N load cell.

Here, $\tau^2 = TL^2/B$ is the dimensionless compressive force (with T the dimensional axial load applied), B is the bending modulus $B = Eh^3b/12$ (with E the Young modulus), ρ_s is the density of the material and $f = FL^2/B$ is the dimensionless indentation force applied at the center of the beam. Time is non-dimensionalized by $t_* = L^2\sqrt{12\rho_s hb/Eh^3b} = 2\sqrt{3}L^2/ch$, with $c = \sqrt{E/\rho_s}$ the sound speed within the material.

The out-of-plane deflection w is coupled to the in-plane horizontal displacement u by Hooke's law relating the compressive stress to the higher-order von Kármán strain. In dimensionless terms, this reads

$$-\mathcal{S}\tau^2 = \frac{\partial u}{\partial x} + \frac{1}{2}\left(\frac{\partial w}{\partial x}\right)^2, \qquad (2)$$

where

$$\mathcal{S} = \frac{B}{EhL^2b} = \frac{h^2}{12L^2}$$

is the "stretchability" of the beam and is a measure of the relative importance of bending and stretching energies. The importance of stretchability has been discussed previously for vibrations about equilibrium within the Kirchhoff formalism [28] and in the context of wrinkling plates [29], though the analytical results and experiments presented here are, to our knowledge, new.

The clamped boundary conditions at the two ends of the arch are given by $w(\pm 1/2) = w'(\pm 1/2) = 0$ while the horizontal compression is imposed by the condition $u(\pm 1/2) = \mp d/2$, where $d = \Delta L/L$ is the dimensionless end-shortening.

Quasi-static evolution. – To study the deformation prior to snapping we assume that loading occurs quasi-statically and consider time-independent solutions of (1), *i.e.* we neglect the $\partial_t^2 w$ term. It is possible to solve the quasi-static equation for the shape of the indented beam analytically, the unknown indentation force f being determined in terms of w_0 as part of the solution (for details, see ref. [30]).

Our analysis reveals that the form of deformation depends on the value of $d/\mathcal{S}$. First, if $d/\mathcal{S} < 4\pi^2$, the compressed, unbuckled beam is stable; neither buckling nor snapping occur as the in-plane compression does not induce Euler buckling in the beam. This can be understood in physical terms as follows: a compression ΔL corresponds to a strain d, a stress Ed or a compressive force $Ehbd$ on the beam. However, the buckling load for a beam with clamped edges is well known to be $F = 4\pi^2 B/L^2 = 4\pi^2\mathcal{S}Ehb$; hence when $d < 4\pi^2\mathcal{S}$ buckling cannot occur. In what follows the quantity $d - 4\pi^2\mathcal{S}$ frequently occurs and should be interpreted physically as the end-end compression that remains after some of the applied confinement of the beam has been accommodated by compressing the beam in response to the buckling load.

If $4\pi^2 < d/\mathcal{S} < \tau_{\max}^2 \approx 80.76$ (with $\tau_{\max} \approx 8.99$ the solution of $\tau_{\max}/2 = \tan(\tau_{\max}/2)$), the arch remains symmetrical as it deforms, ultimately returning to the compressed flat state $w = 0$ (at which point snapping is observed experimentally).

For $d/\mathcal{S} > \tau_{\max}^2 \approx 80.76$, an asymmetric mode appears, in addition to the symmetric mode, once the indentation reaches a critical value or, equivalently, a critical force. Detailed calculations [30] show that this asymmetric mode is energetically favourable whenever it exists. In the asymmetric mode, the force-displacement relation is linear, $f = -207.75 w_0$, and the compressive force τ remains constant at $\tau = \tau_{\max} \approx 8.99$. The FvK analysis also shows that the critical indentation force is given by

$$f^{(c)} = -207.75 w_0^{(c)} = -129.53(d - 80.76\mathcal{S})^{1/2}. \qquad (3)$$

While the theory could be tested by comparing theoretical and experimental beam shapes, a more rigorous test is to compare the force-displacement relationship predicted theoretically with that measured experimentally for each of the three regimes discussed above. In experiments, we have used beams with two different stretchabilities: $\mathcal{S}_1 = 1.912 \times 10^{-4}$ and $\mathcal{S}_2 = 9.706 \times 10^{-4}$. The regime of buckled beams with small compression ($4\pi^2 < d/\mathcal{S} < \tau_{\max}^2 \approx 80.76$) is somewhat difficult to explore experimentally since the weight of the beam becomes important in this case. Therefore, to explore the force-displacement relation for arches in this regime we use the beam with relatively high stretchability ($\mathcal{S}_2 = 9.706 \times 10^{-4}$); the force-displacement plot in this case is shown in fig. 2(b). For the regime of large compression, $d/\mathcal{S} > \tau_{\max}^2 \approx 80.76$, no such restriction applies; a comparison of theory and experiment in this regime, for two different values of $d/\mathcal{S}$, is shown in fig. 2(c).

Note that finite stretchability plays a crucial role in the picture outlined above. First, if stretchability is neglected, $\mathcal{S} = 0$, then the family of beam shapes that return to a flat, compressed beam at $w_0 = 0$ (observed when $d < \tau_{\max}^2\mathcal{S}$) cannot occur. Second, even when $d/\mathcal{S} > \tau_{\max}^2$ the critical transition force between symmetric and asymmetric deformations predicted in (3) is sensitive to the amount of stretchability, as is also seen experimentally (fig 2(d)). It is in only in the high arch regime that stretchability becomes negligible [26].

One final result from the study of the quasi-static indentation of an arch visible in fig. 2(b), (c) is vital for our study of snapping: regardless of which deformation mode occurs, *i.e.* independently of the precise value of $d/\mathcal{S}$, the indentation force and w_0 vanish together. This is also similar to what is observed in the confinement of a buckled arch in a shrinking box [31,32]. If $4\pi^2 < d/\mathcal{S} < \tau_{\max}^2$, the solution at this point is the flat compressed beam, while for $d/\mathcal{S} > \tau_{\max}^2$, the beam has the form of the antisymmetric, mode-2 Euler buckling. In both cases, if the indentation were to continue, symmetry dictates that the indentation force would have to become negative. In the absence of any adhesion between indentor and arch, this is not possible and so no equilibrium solution is possible —contact must be lost and the beam must then "snap-through" to the

stable state, the inverted arch. This explains the experimental observation that snap-through occurs when the neutral axis of the beam is displaced to the mid-point of the clamped edges.

Dynamics of snapping and ringing. – To understand the timescale of the snap-through, we perform a linear stability analysis of the beam at the point at which contact with the indentor is lost. We set $f = 0$ in eq. (1) and look for solutions of the form $w(x,t) = w_\alpha(x) + \epsilon w_p(x) e^{\sigma t}$, where $w_\alpha(x)$ is the shape at the point of snapping ($\alpha = 0, 2$ depending on whether snapping occurs from the flat or asymmetric modes). We also perturb the compressive force, $\tau = \tau_\alpha + \epsilon \tau_p e^{\sigma t}$. At leading order in ϵ we obtain an eigenvalue problem for the growth rate σ with eigenfunction $w_p(x)$ satisfying

$$\frac{\mathrm{d}^4 w_p}{\mathrm{d}x^4} + \tau_p^2 \frac{\mathrm{d}^2 w_p}{\mathrm{d}x^2} + \sigma^2 w_p = -2\tau_\alpha \tau_p \frac{\mathrm{d}^2 w_\alpha}{\mathrm{d}x^2}, \qquad (4)$$

$$\int_{-1/2}^{1/2} \frac{\mathrm{d}w_\alpha}{\mathrm{d}x} \frac{\mathrm{d}w_p}{\mathrm{d}x} \mathrm{d}x = -2\mathcal{S}\tau_\alpha \tau_p, \qquad (5)$$

along with boundary conditions $w_p(\pm 1/2) = w_p'(\pm 1/2) = 0$. The eigenproblem (4),(5) can be reduced to the solution of a transcendental equation for σ. Here, we summarize the results of this analysis giving details in the supplementary information [30].

For $4\pi^2 < d/\mathcal{S} < \tau_{\max}^2$, for which the arch snaps from the compressed flat mode ($\alpha = 0$), analytical insight may be obtained by considering compressions just large enough to obtain buckling, *i.e.* $(d/\mathcal{S})^{1/2} \gtrsim \tau_0 = 2\pi$. In this limit we find

$$\sigma \approx \frac{4\pi^{3/2}}{\sqrt{3}} \left[\left(\frac{d}{\mathcal{S}} \right)^{1/2} - 2\pi \right]^{1/2}. \qquad (6)$$

For snap-through from the asymmetric mode ($\alpha = 2$) there is a single eigenvalue of the system, $\sigma \approx 24.113$, that is independent of the end-shortening d and stretchability $\mathcal{S}$. Thus, if we fix $\mathcal{S}$ and increase d starting from $d = 4\pi^2\mathcal{S}$, the growth rate increases monotonically from zero until $d = \tau_{\max}^2 \mathcal{S}$, at which point the growth rate plateaus and snap-through happens from the asymmetric mode. Numerical solutions of the Kirchhoff equations confirm a similar picture, though for $d/\mathcal{S} > \tau_{\max}^2$ there is, in fact, a small dependence of σ on $d/\mathcal{S}$, consistent with values reported in a related problem [26].

Experimentally, we tracked the motion of the center of the beam with a high-speed camera (Photron FASTCAM APX RS, @3000 fps) and performed image analysis with imageJ and custom MATLAB scripts to study the change in displacement with time. Figure 3 shows that as the center point reaches the base of the arch it rapidly moves from point A to point B, corresponding to the "snap-through". The beam then vibrates like an under-damped oscillator about the "inverted" symmetrical shape before coming to rest. In the inset of fig. 3 we plot the absolute value of the central deflection between points A and B; this plot shows that $|w_0|$ grows approximately exponentially with time so that a growth rate can be measured. We non-dimensionalize the experimentally obtained growth rate using the timescale $t_* \sim L^2/ch$ that arises naturally from the dynamic beam equation; fig. 4 shows that the timescale of the snap-through observed experimentally agrees well with theoretical predictions. In particular, the growth rate σ is strongly dependent on the degree of confinement for $4\pi^2 < d/\mathcal{S} < \tau_{\max}^2$, as predicted by eq. (6), but once $d/\mathcal{S}$ crosses the critical value $d/\mathcal{S} = \tau_{\max}^2 \approx 80.76$, confinement plays a negligible role and $\sigma \approx 24.113$.

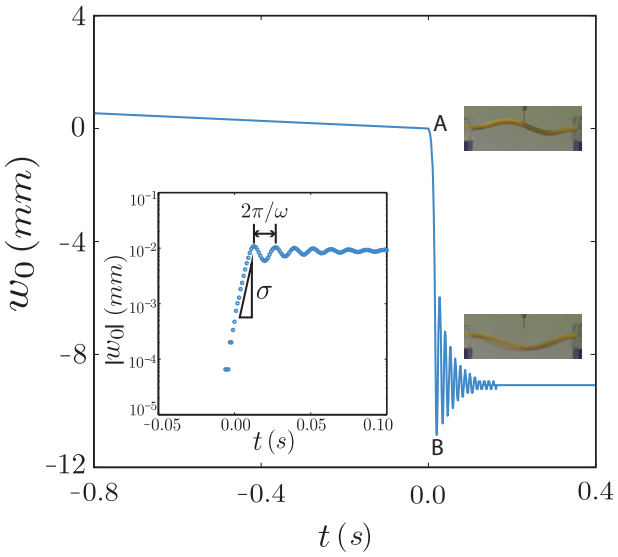

Fig. 3: (Colour on-line) Dynamics of arch snap-through. Main figure: experimentally measured displacement of the central point as the arch snaps and vibrates. Inset: semilog plot of displacement *vs.* time, showing the growth rate σ and vibration frequency ω after snapping.

Having snapped away from its unstable configuration, the beam approaches the inverted arch state, which is a stable equilibrium. Since there is little dissipation in our system, the beam oscillates about this state. To understand the "ringing" frequency $\omega = \sqrt{-\sigma^2}$ of this vibration we perform a linear stability analysis as before, but now with $w_\alpha = w_1$, the stable, first Euler buckling mode. Here, we again see a transition in the form of oscillation based on the quantity $d/\mathcal{S}$. Starting at the critical value $d/\mathcal{S} = 4\pi^2$, as $d/\mathcal{S}$ is increased the ringing frequency of the lowest mode of oscillation increases. The FvK model predicts that

$$\omega \approx \frac{2^{3/2}\pi}{3^{1/2}} \left(\frac{d}{\mathcal{S}} - 4\pi^2 \right)^{1/2} \qquad (7)$$

for $d/\mathcal{S} \gtrsim 4\pi^2$. The Kirchhoff model confirms this result for $d/\mathcal{S} \approx 4\pi^2$ and shows that ω continues to increase up to $\omega \approx 42.38$ when $d/\mathcal{S} = 122.4$. For $d/\mathcal{S} > 122.4$, the frequency of the lowest mode is fixed at $\omega \approx 42.38$, independent of $d/\mathcal{S}$. We also see a transition in the form

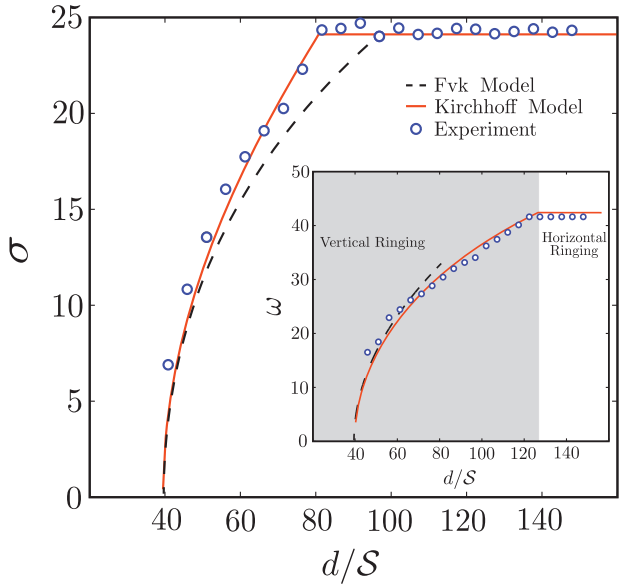

Fig. 4: (Colour on-line) Variation of growth rate σ with rescaled lateral confinement, $d/\mathcal{S}$. Inset: the "ringing" frequency ω as a function of $d/\mathcal{S}$. The results of numerical simulations (solid curves) and experiments (points) are in good agreement with one another and with the prediction of the FvK model (6), (7) (dashed curves) for $d/\mathcal{S} \approx 4\pi^2$.

of oscillation. For $d/\mathcal{S} < 122.4$, the mode of oscillation with the lowest frequency corresponds to a vertical oscillation, whereas for $d/\mathcal{S} > 122.4$ the mode with lowest frequency also has a significant horizontal component. To compare this picture with experimental data the Fourier transform of the displacement data was taken to measure the frequency of the vibrations after snapping; fig. 4, inset, shows good agreement between the experiments and theory. The post-snap ringing timescale of the beam ($t_r^{(b)}$) for $d/\mathcal{S} > 122.4$ is governed by the geometry and material properties of the arch:

$$t_r^{(b)} = (2\pi/\omega)t_* \approx 0.148t_* \approx 0.513L^2/ch. \qquad (8)$$

Ringing of spherical shells. – The audible pop that accompanies the snapping of toys, such as jumping discs [15] and the popper shown in fig. 1, can be attributed to the ringing frequency. It is therefore natural to compare the ringing timescale (8) with that for a spherical cap. The analogue of the beam length for a spherical cap is the base diameter, which we therefore denote by $L_{\rm base}$. For an elastic spherical cap with radius of curvature R and thickness h, the analogue of the FvK equation (1) is the dynamic Donnell-Mushtari-Vlasov equation [33], which reads, in dimensional terms

$$\rho_s h\frac{\partial^2 w}{\partial t^2} + B\nabla^4 w + \frac{Eh}{R^2}w = 0, \quad 0 \le r \le L_{\rm base}/2, \qquad (9)$$

where $B = Eh^3/12(1-\nu^2)$ is the appropriate bending stiffness (with Poisson ratio ν), r is the radial coordinate, and we shall assume axisymmetry in what follows.

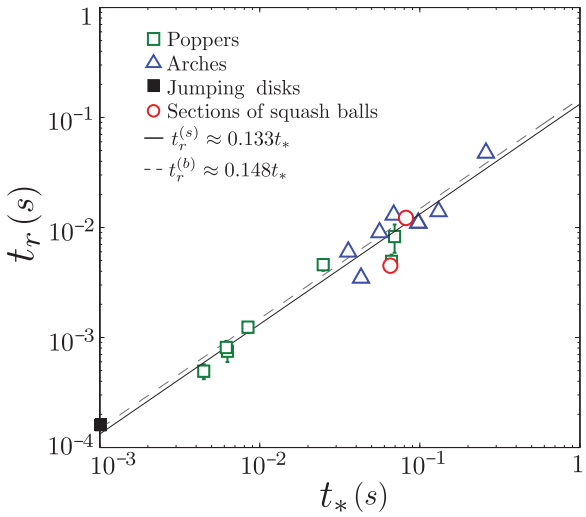

Fig. 5: (Colour on-line) The ringing timescale measured experimentally, t_r, scales with the timescale t_* as predicted by our analysis for arches, $t_r^{(b)} \approx 0.148t_*$ and for hemispherical shells $t_r^{(s)} \approx 0.133t_*$.

Once a popper has leapt from a table, its edges are free and so the appropriate boundary conditions for (9) are $\nabla^2 w|_{r=L_{\rm base}/2} = \mathrm{d}/\mathrm{d}r(\nabla^2 w)|_{r=L_{\rm base}/2} = 0$. Performing a linear stability analysis along similar lines to those for the snapping beam (see supplementary information [30] for more details) we obtain the snapping timescale

$$t_r^{(s)} = \frac{\pi}{2}\frac{\sqrt{1-\nu^2}}{\lambda^2}t_*\left(1+\frac{3}{4}\frac{1-\nu^2}{\lambda^4}\frac{{L_{\rm base}}^4}{h^2R^2}\right)^{-1/2}, \qquad (10)$$

where $\lambda \approx 3.196$ is an eigenvalue that is found numerically from a solvability condition.

For the majority of the shells of interest here, the term in parentheses in (10) is approximately unity and we find, assuming $\nu \approx 1/2$, that $t_r^{(s)} \approx 0.133t_*$. Remarkably, we find that this result is within 10% of the corresponding result for the ringing frequency of arched beams in (8). Given the quantitative robustness of the ringing timescale, it is natural to measure its value in a wide range of experiments combining the snapping shells that motivated our study with the carefully controlled snapping beams. For spherical shells (commercially available toy poppers, bimetallic disks and sections of squash balls) we measure with a microphone the audible "pop" sound that they make during snapping and extract the dimensional frequency, ω/t_* from this. The lengthscale used to estimate t_* is the uncompressed length L for arches and $L_{\rm base}$ (the diameter of the spherical cap base) for hemispherical shells. Figure 5 shows plots of the experimentally measured ringing timescale, t_r, as a function of the characteristic timescale t_*; this confirms that the prediction of the linear stability analysis for both beams and shells is in excellent agreement with experiments.

Conclusions. – We have studied the dynamic snapping of beams and shells. By first analyzing the

quasi-static deformation of a point-loaded beam, we established the key role of stretchability in the small end-end compression regime, and showed that for $4\pi^2\mathcal{S} < d < 80.76\mathcal{S}$ the static deformation and dynamic snapping are fully symmetric, a regime that ceases to exist in the inextensible limit $S \to 0$. However, we emphasize that this is not a generic feature of such systems; the loading also plays a crucial role since when indenting with a flat wall, the arch remains symmetric throughout the deformation independent of the stretchability [31,32].

Interestingly, our analysis and experiments showed that stretchability of the beam also plays a key role in determining the timescales that govern both snap-through and ringing. More generally, we found that the characteristic timescale in each case $\sim L^2/ch$, which may be interpreted physically as the timescale for the beam to "feel" its ends using sound waves of speed c, augmented by a geometric factor L/h. The augmenting factor, $L/h \sim \mathcal{S}^{-1/2}$, so that for a given stretchability $\mathcal{S}$ it is the time taken to "feel" the beam ends that limits the dynamics of motion. For shells, we showed that the timescale of ringing scales in the same way with the shell's properties and, moreover, with a very similar prefactor. This allowed us to present a universal description for the audible "pop" that is a distinctive feature of snapping both in everyday toys and laboratory experiments.

While our results have demonstrated that the ringing of arches and shells are quantitatively similar, many open questions remain to properly understand the dynamics of snapping structures. A particularly interesting open question concerns the effect of finite stretchability in determining the snapping growth rate for shells and whether such effects manifest themselves in terms of the symmetry (or asymmetry) of the snapping mode, as we have seen for snapping beams.

* * *

We are grateful to Howard Stone (Princeton) for his hospitality during the Oxford-Princeton Collaborative Workshop Initiative 2013, and the participants of that workshop, for useful suggestions in the completion of this work. DV is partially supported by a Leverhulme Trust Research Fellowship. AP and DPH acknowledge the financial support from NSF through CMMI-1300860.

REFERENCES

[1] Gordon J. E., *Structures or Why Things Don't Fall Down* (Penguin Books Ltd.) 1978.
[2] Hurlbrink E., *Schiffbau*, **9** (1908) 517.
[3] Timoshenko S. P., *Bull. Polytech. Inst. Kiev* (1910).
[4] Fung Y. and Kaplan A., *National Advisory Committee for Aeronautics*, NACA report (1952), pp. 1–76.
[5] Gjelsvik A. and Bodner S., *ASCE Proceedings, J. Eng. Mech. Div.*, **88** (1962) 87.
[6] Pippard A. B., *Eur. J. Phys.*, **11** (1990) 359.
[7] Patrício P., Adda-Bedia M. and Ben Amar M., *Physica D*, **124** (1998) 285.
[8] Pi Y. L., Bradford M. A. and Uy B., *Int. J. Solids Struct.*, **39** (2002) 105.
[9] Plaut R. H. and Virgin L. N., *J. Appl. Mech.*, **76** (2009) 041011.
[10] Poppinga S. and Joyeux M., *Phys. Rev. E*, **84** (2011) 041928.
[11] Forterre Y., Skotheim J. M., Dumais J. and Mahadevan L., *Nature*, **433** (2005) 421.
[12] Skotheim J. M. and Mahadevan L., *Science*, **308** (2005) 1308.
[13] Wittrick W. H., Myers D. M. and Blunden W. R., *Q. J. Mech. Appl. Math.*, **6** (1953) 15.
[14] Lapp D. R., *Phys. Educ.*, **44** (2008) 492.
[15] Ucke C. and Schlichting H.-J., *Phys. Educ.*, **44** (2009) 612.
[16] Hsu C. and Hsu W., *J. Micromech. Microeng.*, **13** (2003) 955.
[17] Das K. and Batra R. C., *Smart Mater. Struct.*, **18** (2009) 115008.
[18] Goncalves P., *Int. J. Solids Struct.*, **40** (2003) 5017.
[19] Holmes D. P. and Crosby A. J., *Adv. Matter*, **19** (2007) 3589.
[20] Xia C., Lee H. and Fang N., *J. Micromech. Microeng.*, **20** (2010) 085030.
[21] Panesar A. S., Hazra K. and Weaver P. M., *Composites, Part A*, **43** (2012) 926.
[22] Thill C., Etches J., Bond I., Potter K. and Weaver P., *Aeronaut. J.*, **112** (2008) 117.
[23] Libai A. and Simmonds J. G., *The Nonlinear Theory of Elastic Shells* (Cambridge University Press) 1998.
[24] Humphreys J. S., *AIAA J.*, **4** (1966) 878.
[25] Pi Y.-L. and Bradford M. A., *Nonlinear Dyn.*, **73** (2013) 1289.
[26] Fargette A., Neukirch S. and Antkowiak A., arXiv:1307.1775 [cond-mat.soft] (2013).
[27] Audoly B. and Pomeau Y., *Elasticity and Geometry* (Oxford University Press) 2010.
[28] Neukirch S., Frelat J., Goriely A. and Maurini C., *J. Sound Vib.*, **331** (2012) 704.
[29] Hure J., Roman B. and Bico J., *Phys. Rev. Lett.*, **109** (2012) 054302.
[30] Pandey A., Moulton D. E., Vella D. and Holmes D. P., arXiv:1310.3703 [cond-mat.soft] (2013).
[31] Roman B. and Pocheau A., *Europhys. Lett.*, **46** (1999) 602.
[32] Roman B. and Pocheau A., *J. Mech. Phys. Solids*, **50** (2002) 2379.
[33] Soedel W., *Vibrations of Shells and Plates* (Marcel Dekker) 2004.